Steric crowding of a series of pyridine based ligands influencing the photophysical properties of Zn(II) complexes†

Daniel Ejarque, [ID a] Teresa Calvet,[b] Mercè Font-Bardia[c] and Josefina Pons [ID *a]

[a] Departament de Química, Universitat Autònoma de Barcelona, 08193-Bellaterra, Barcelona, Spain. E-mail: josefina.pons@uab.es

[b] Departament de Mineralogia, Petrologia i Geologia Aplicada, Universitat de Barcelona, Martí i Franquès s/n, 08028 Barcelona, Spain

[c] Unitat de Difracció de Raig-X, Centres Científics i Tecnològics de la Universitat de Barcelona (CCiTUB), Universitat de Barcelona, Solé i Sabarís, 1-3, 08028 Barcelona, Spain

ABSTRACT

$Zn_{(II)}$ complexes containing N, N,N and N,N,N pyridine (dPy) ligands tend to display improved fluorescence efficiencies in comparison with their starting ligands benefiting from the chelation enhanced effect (CHEF) and preventing photoinduced electron transfer (PET) mechanisms by the coordination of their lone pair electrons. Nevertheless, the size of $Zn_{(II)}$ makes steric crowding an important factor to be considered, since it can promote the elongation of the coordination bonds that weakens their strength and favors the reduction of fluorescence efficiencies through PET processes. For that reason, in this contribution we have performed a systematic study of $Zn_{(II)}$ compounds based on α-acetamidocinnamic acid (HACA) and a comprehensive range of dPy ligands with increasing bulkiness (pyridine (py) (1), 3-phenylpyridine (3-phpy) (2), 2,2'-bipyridine (2,2'-bipy) (3), 1,10-phenanthroline (1,10-phen) (4), 2,2':6',2''-terpyridine (terpy) (5) and 4'-(4-methylphenyl)-2,2':6',2''-terpyridine (mpterpy) (6)), which has allowed the equilibrium between CHEF and steric crowding effects to be studied. The elucidation of the six crystal structures revealed the formation of one coordination polymer (1) and five monomeric complexes (2–6). All of them have been characterized by analytical and spectroscopic techniques, and their molecular and supramolecular structures have been discussed. Furthermore, the UV-vis and photoluminescence properties have been recorded and their quantum yield (Φ) values have been calculated. Finally, it has been observed that even though the CHEF has a favorable impact on the fluorescence properties, the steric crowding of the ligands has been imposed, leading to fluorescence quenching.

INTRODUCTION

The design of coordination complexes has become a promising research area during the last decades due to their structural diversity and their applications in sensing,1 magnestism,[2] luminescence,[3,4] and so on.[5,6] A common strategy for synthesizing these complexes is the self-assembly of ligands with metal ions for obtaining desired products bearing in mind that there are many factors to be considered, such as the metal salts,[7] the metal–ligand ratio,[8] the bulkiness of the ligands,[9] the solvent,[10] the synthetic method,[11] among others.[12,13]

Since the coordination of organic ligands to metal ions offers extra rigidity to the resulting products, this effect has been used for obtaining complexes with improved photophysical properties. Furthermore, discrete units (0D) and linear coordination polymers (1D) have received increasing interest because of their better solvent processability in comparison with 2D and 3D metal–organic materials.[14–17] Therefore, numerous studies about coordination complexes and the effect of their ligands in the quantum yield (Φ)[18] have been performed in order to understand them.[19–22] Indeed, the rigidity provided by the formation of coordination bonds presents the advantage of preventing energy loss through bond vibrations and photoinduced electron transfer (PET) processes.[23] Moreover, d^{10} metal centers are especially suitable for the preparation of fluorescent coordination complexes not only due to their zero crystal field stabilization energy (CFSE), but also due to their absence of potential quenching processes derived from d–d transitions. Therefore, only ligand-centered (LC) and/or ligand-to-metal charge transfer (LMCT) excited states are allowed.[24–28]

The use of Zn(II) complexes has been especially employed in combination with pyridine ligands because of their good fluorescence efficiency exploiting their chelation enhanced effect (CHEF).[29,30] Moreover, the bioavailability of Zn(II) complexes makes them appropriate for biological applications.[6] Notwithstanding, the size of Zn(II) ions (NC(4) = 0.60 Å; NC(5) = 0.68 Å; NC(6) = 0.74 Å)31 enables the steric crowding effect to play an important role in the photophysical properties. This effect leads to the elongation of coordination bonds (Zn–L) promoting their weakening and therefore, decreasing the CHEF and favoring the quenching of fluorescence through PET mechanisms.[32–34] Therefore, the study of the distortion of the Zn(II) cores is essential for understanding their luminescence properties and being able to modulate them, since there is an equilibrium between the CHEF and steric crowding effects, which needs to be studied to find the better steric requirements for each Zn(II) system.

Previously, our group studied the reactivity of p-hydroxycinnamic acid towards Cu(II).[35] Afterwards, we continued this research with another cinnamic acid derivative ligand namely α-acetamidocinnamic acid (HACA), whose reactivity towards Zn(II) and Cd(II) was analyzed, observing the formation of isostructural monomeric compounds. Furthermore, their reactivity in the presence of 4-phenylpyridine (4-phpy) shows a different behavior between Zn(II) and Cd(II), obtaining a monomeric complex and a dimeric complex. The photophysical properties of these complexes were recorded, observing the higher efficiency of Cd(II) over Zn(II) complexes and the quenching effect of 4-phpy with both metal centers.[36] Notwithstanding, the ACA ligand presents a conjugated system with four different coordination points, which could be a suitable candidate for exhibiting promising photophysical properties, especially when the acetamide moiety gets tied up for avoiding nonradiative decay processes.

Within this frame, in this contribution we have studied the effect of adding different N, N,N and N,N,N pyridine (dPy) ligands with increasing bulkiness and the relationship between the

steric crowding generated by these ligands and the photophysical properties of the resulting compounds. For the selection of the dPy ligands, three main factors have been considered: (a) their aromatic nature; (b) their increasing denticity (N, N,N and N,N,N), which will stabilize their coordination and thus, will emphasize the CHEF effect; and (c) their increasing bulkiness to avoid solvent attack and therefore, prevent the solvent quenching of fluorescence. For that reason, the dPy ligands selected for this work were two N donors (pyridine, py; 3-phenylpyridine, 3-phpy), two N,N donors (2,2'-bipyridine, 2,2'-bipy; 1,10-phenanthroline, 1,10-phen) and twoN,N,N donors (2,2':6',2''-terpyridine, terpy; 4'-(4-methylphenyl)-2,2':6',2''-terpyridine, mpterpy). From the reactions of $Zn(OAc)_2 \cdot 2H_2O$, HACA and the corresponding pyridines, we successfully isolated one coordination polymer (CP) and five monomeric complexes: $[Zn(\mu\text{-}O,O'\text{-}ACA)(ACA)(py)]_n$ (1), $[Zn(ACA)_2(3\text{-}phpy)_2] \cdot EtOH$ (2), $[Zn(ACA)_2(2,2'\text{-}bipy)] \cdot 4EtOH$ (3), $[Zn(ACA)_2(1,10\text{-}phen)][Zn(ACA)_2(1,10\text{-}phen)] \cdot 3EtOH$ (4), $[Zn(ACA)_2(terpy)] \cdot 2DMF$ (5) and $[Zn(ACA)_2(mpterpy)] \cdot 4MeOH$ (6) (Scheme 1). These complexes were fully characterized, and their crystal structures were elucidated. Finally, the photophysical properties were studied and the steric effects of the dPy ligands were related with the Φ values.

RESULTS AND DISCUSSION

Synthesis and characterization

Compounds 1–6 were prepared via combination of $Zn(OAc)_2{\cdot}2H_2O$, HACA and py (1), 3-phpy (2), 2,2′-bipy (3), 1,10-phen (4), terpy (5) and mpterpy (6) in a 1 : 2 : 1 molar ratio, using EtOH as solvent at room temperature (RT). The corresponding crystals suitable for X-ray crystallographic analysis were grown by diverse methods such as synthesis starting from small quantities of reagents (1), RT evaporation of mother liquors (2 and 4), recrystallization in different solvents (3 and 5) and layering techniques (6). The diversity of the solvents obtained arises from the different solvents used for the crystallization of the products. Further details of the synthetic methodologies and the synthesis of the single crystals are provided in the ESI† (Exp. Sec.).

All the compounds were characterized by elemental analysis (EA), FTIR-ATR, ^{1}H, $^{13}C\{1H\}$ and DEPT-135 NMR spectroscopies and single crystal X-ray diffraction method. Finally, the UV-vis and photoluminescence spectra of the six complexes were recorded and their Φ values were calculated. Detailed information is provided in the Experimental section.

The EA of compounds 1–6 agree with the proposed formula. In the FTIR-ATR spectra, the absence of a broad band between 2704 and 2405 cm^{-1} corresponding to $\nu(O–H)_{HACA}$ and a strong peak at 1637 cm^{-1} attributable to $\nu(COOH)_{HACA}$ indicate that the HACA is deprotonated in the six complexes. The spectra show the characteristic carboxylate bands in the range of 1607–1518 cm^{-1} for $\nu_{as}(COO)$ and 1415–1365 cm^{-1} for $\nu_{s}(COO)$ (ESI:† Fig. S1–S6). The difference between these bands [$\Delta = \nu_{as}(COO) - \nu_{s}(COO)$] is 135 and 215 (1), 208 (2), 108 (3), 205 and 113 (4), 222 (5) and 229 (6) suggesting monodentate (1, 2, 4, 5 and 6) and bidentate chelating (1, 3, and 4) coordination modes of the carboxylate groups.[37,38] All of the Δ values agree with the data obtained from the crystal structures. In addition, some specific groups of the ACA ligand such as the NH and C=O groups can be identified through the ν(N–H) and ν(C=O) bands in all of the spectra, as well as the $\nu(C–H)_{ar}$, ν(C=C/C=N), δip(C–H) and δ_{oop}(C–H) bands from the aromatic rings.[39] Furthermore, the presence of solvent molecules allows further identification of some specific bands in 2–6. For 2–4 and 6, broad bands between 3640 and 3370 cm^{-1} were observed corresponding to ν(O–H) bands, suggesting the presence of solvent molecules. In addition, in 5, the ν(C=O) band attributable to the presence of DMF is observed.

The ^{1}H NMR spectra of 1–6 were recorded in dmso-d6 solutions (ESI:† Fig. S7–S12). The spectra of the six complexes show a signal attributable to the NH of ACA at 9.29–8.96 ppm, while the signals of the aromatic protons from ACA appear between 7.51 and 7.22 ppm. Moreover, after the signals of the aromatic ACA protons, a signal between 7.29 and 7.10 ppm corresponding to the alkene proton is observed. The bands corresponding to the aromatic protons of each dPy are also observed between 9.10 and 7.42 ppm. Finally, the methyl protons appeared between 1.97 and 1.84 ppm, while the methyl protons of mpterpy in 6 appear at 2.44 ppm. The ^{1}H NMR spectra of 1–6 confirm their 1 ACA : 1 dPy (2) or 2 ACA : 1 dPy (1 and 3–6) molar ratio.[39]

The $^{13}C\{^{1}H\}$ and DEPT-135 NMR spectra of 1–6 have also been recorded in dmso-d_6 solutions (ESI:† Fig. S13–S18). The spectra of the six complexes display the band assignable to the carbon atom of the carbonyl group between 170.67 and 169.18 ppm, while the carbon atom from the carboxylate group appears between 168.48 and 167.85 ppm. The carbon atoms from

the different pyridine ligands are also observed between 153.05 and 118.89 ppm. In this region, the two carbon atoms from the double bond of the ACA are also observed and appear separately, at 135.42–135.04 ppm for the quaternary carbon and at 128.21–127.18 ppm for the remaining one. Moreover, the aromatic protons from ACA are located between 130.54 and 129.13 ppm. The methyl carbon atom from the ACA is found to be between 23.08 and 22.98 ppm, while the methyl carbon of mpterpy in 6 appears at 20.95 ppm.

Crystal and extended structures of complex 1

Complex 1 crystallizes in the monoclinic $P2_1/n$ space group and consists of a Zn(II) zigzag polymeric structure, expanding through a bridging ACA via carboxylate and carbonyl groups along the b axis. The metal center presents a square pyramidal [ZnO_4N] core composed of two ACA and one py ligand. The carboxylate groups of the ACA show a monodentate and a bidentate chelating coordination mode, the latter being responsible for the extension of the polymeric array through the bridging carbonyl of the acetamide moiety (Fig. 1a). This behavior of the carbonyl group in ACA has been previously observed by our group in another coordination polymer containing 4-phenylpyridine.[40]

The distinction of the geometry between trigonal bipyramidal and square pyramidal is evaluated through the τ_5 parameter.[41] The value of τ_5 for 1 is 0.37 indicating a highly distorted square pyramidal geometry with bond angles between 55.80(7) and 149.6(1)° and bond lengths between 1.956(2) and 2.122(3) Å. In addition, there is another Zn–O bond with a distance of Zn1–O2 = 2.570(2) Å, which is considered as a weak coordination bond (Table 1).[42] These values are in the range of those of other $Zn_{(II)}$ complexes containing coordinated carboxylates, carbonyls and pyridine ligands.[40,43,44]

The polymeric array of 1 is supported by additional intramolecular interactions based on N–H···$O_{C=O}$ interactions between contiguous amide moieties and π···π interactions between ACA and py aromatic rings. Furthermore, there are other weaker C–H···O interactions involving the same oxygen atom from the carbonyl moiety as the N–H···$O_{C=O}$ interaction and an oxygen atom from a carboxylate group (Fig. 1b; ESI:† Table S1).

The intermolecular interactions of 1 associate the chains by two H-bonds. One of them joins the amide moieties with the uncoordinated oxygen atoms of the monodentate ACA, expanding the structure in the [101] direction (Fig. 1c). The second interaction associates the p-H atoms of the monodentate ACA with the oxygen atoms from the bidentate chelating carboxylate groups, expanding the structure through the a direction (Fig. 1d). All of these interactions expand the structure forming a 3D supramolecular network.

Crystal structure of complexes 2–6

Compounds 2–6 consist of $Zn_{(II)}$ monomeric structures crystallizing in the monoclinic C2/c (2), $P2_1/c$ (3), and C2/c (5); orthorhombic $Pca2_1$ (4); triclinic $P1^-$ (6) space groups. The crystal structure of 4 shows two crystallographically independent monomeric units (4a and 4b). Additionally, all of the structures contain occluded solvent molecules (EtOH (2–4); DMF (5) and MeOH (6)). The structures have [ZnO_2N_2] (2), [ZnO_3N_2] (4a, 5 and 6) and [ZnO_4N_2] (3, 4b) cores, all of them composed of two ACA ligands and one dPy, except for 2, which has two 3-phpy

ligands. Besides, the ACA ligands present monodentate (2, 5 and 6), bidentate chelating (3 and 4b) or a combination of monodentate and bidentate chelating (4a) coordination modes (Fig. 2).

The distortion on the geometry of the four, five and sixcoordinated species is determined by the τ_4,[45] τ_5 [41] and average twist angle (ata)[46,47] parameters. For 2, the τ_4 value is 0.87 indicating a distorted tetrahedral geometry with bond angles between 98.3(1) and 122.7(1)° (Table 1), and the Zn–O and Zn–N bond lengths lie within the usual values for similar $Zn_{(II)}$ tetrahedral species.[48,49] Moreover, the τ_5 parameter for 4a, 5 and 6 is 0.41, 0.37 and 0.28, respectively, showing distorted square pyramidal geometries with bond angles between 61.0(1) and 154.6(2)° (4a), 76.23(7) and 152.5(2)° (5), and 75.65(9) and 151.97(9)° (6) (Table 2). Their Zn–O and Zn–N bond lengths lie within the range of reported values for five-coordinated complexes.[50–53] Finally, the ata values for 3 and 4b are 31.78° and 46.68°, respectively, indicating octahedral geometries with distortions arising from their bond angles, which range between 61.02(9) and 155.1(1)° (3) and 60.6 (2) and 153.2(2)° (4). Additionally, the Zn–O and Zn–N bond lengths lie in the usual values reported for similar octahedral compounds.[51,54,55]

Extended structure of complexes 2–6

The intermolecular interactions of 2–6 associate the corresponding monomeric units through recurring and reciprocal N–H···O_{COO} interactions in all of the compounds except 5, where weak reciprocal C–H···O_{COO} interactions occur. Furthermore, these interactions are supported by π···π stackings between the aromatic rings of the corresponding dPy ligands in 3, 4 and 6. In addition, different C–H···O interactions also support the expansion through the b axis for the five monomeric compounds.

For 3, 4 and 6, the propagation through a second direction is carried out by contiguous H-bonds involving the occluded EtOH (3 and 4) or MeOH (6) molecules. Additional combinations of C–H···π (2), C–H···O (3 and 6) or π···π (4) interactions form the 3D supramolecular networks, whereas for 5 the presence of C–H···O interactions extends the structure to form 2D layers. Detailed information on the specific intermolecular interactions for all of the complexes are provided in Fig. 3–7 and in the ESI† (Tables S1 and S2).

Structural comparison

The Zn–L bond lengths have been compared to examine the steric crowding effect generated by the ligands around the metal centers in 1–6. For that purpose, the chelate angles of ACA and the bite angles of the pyridine ligands are summarized in Table 3. Moreover, the outer atom angle of the pyridine ligands has also been used, since differently from the chelate and bite angles, it considers the planarity of the linkers and their steric effect by using the two outer hydrogen atoms placed at their sides.[56] The measured parameters show that the py ligand in 1 presents the lowest outer atom angle (80.19°) and thus, permitted the coordination of additional atoms such as the oxygen atom from the carbonyl of the ACA to the metal center. This behavior has also been observed in previous contributions using 4-phpy, which presents similar outer atom angles between 79.42 and 82.42°, permitting the coordination of oxygen atoms from the carbonyl group of the ACA ($[Zn_2(\mu\text{-}O,O'\text{-}ACA)_2(ACA)2(4\text{-}Phpy)_2]n$),[40] the carboxylate group of a nearby ACA through a bridged coordination ($[Zn_3(\mu\text{-}ACA)_6(4\text{-}Phpy)_2]\cdot 4CH_3CN$),[40] or additional coordinated solvent molecules ($[Zn(ACA)_2(4\text{-}phpy)_2(H_2O)_2]\cdot 3H_2O$),[36] yielding polymeric, trimeric and monomeric complexes depending on

the synthetic conditions. Furthermore, the use of 3-phpy, bearing a larger outer atom angle of 94.19°, has driven the formation of monomeric complexes where two 3-phpy coordinate into the metal center. From this point, the N,N and N,N,N pyridine ligands present considerably larger outer atom angles indicating the higher steric hindrance of their coordination into the metal center, and only permitting the introduction of one dPy molecule. The comparison between the N,N ligands show similar outer atom angles for 2,2′-bipy and 1,10-phen even though these values are slightly higher for 3 with respect to 4 (Table 3). For that reason, the monomeric forms 3 and 4b present the same coordination environment formed by two ACA and one pyridine ligand, all of them linked by bidentate chelating coordination modes. Otherwise, the monomeric form 4a displays a pentacoordinated complex, which could be attributed to the higher chelate angle of ACA in 4a with respect to 4b, which only allows the bidentate chelating coordination of one of the ACA ligands. Finally, the N,N,N pyridines in 5 and 6 present the highest outer atom angles being 226.01° (5) and 226.36° (6), owing to the use of the bulkier ligands. These values are very similar because terpy and mpterpy display the same coordination environment, which in both cases restrict the coordination of the ACA to monodentate coordination modes.

Photophysical properties

UV-vis spectroscopy. UV-vis measurements were carried out for 1–6 and their corresponding free ligands in MeOH (3-phpy, 2,2′-bipy, 1,10-phen and terpy ligands) and EtOH (py, mpterpy ligands and 1–6) at 298 K (ESI:† Fig. S19–S32). The procedure followed consists of recording continuous measurements of each sample starting from $\sim 1.00 \times 10^{-9}$ M solutions and increasing the concentration until $\sim 1.00 \times 10^{-4}$ M, to determine at which concentrations the aggregation occurs. Then, the photoluminescence measurements for all of the complexes and ligands were carried out at the suitable concentration to avoid possible aggregation-caused quenching (ACQ).[57] The complexes start to aggregate at 4.74×10^{-7} M (1), 4.50×10^{-7} M (2), 3.49×10^{-7} M (3), 2.00×10^{-7} M (4), 3.92×10^{-7} M (5) and $8.75 \times 10^{-}8$ M (6). Within this range of concentrations, all of the complexes show a bathochromic shift, corresponding to the formation of J-aggregates based on head-to-tail planar interactions.[58,59] These results agree with the structural description since the formation of parallel planar interactions is prevented by the steric hindrance of the monomeric units. Additionally, the study of the supramolecular structures revealed that those complexes forming head-to-tail π···π stackings (3, 4 and 6) are the ones that aggregate at lower concentrations (6 > 4 > 3 > 5 > 2 > 1). The UV-vis spectra of 1–6 using a concentration of $\sim 2 \times 10^{-7}$ M can be found in the ESI† (Fig. S33), showing that molar absorptivities (ε) increase in the order: 1 < 2 < 3 < 6 < 4 < 5. For all of the complexes, the spectra show a band at ~201 nm attributable to metal-toligand (MLCT) or ligand-to-metal (LMCT) charge transfer transitions, and a second band at 271–279 nm, which could be associated with ligand centered (LC) transitions involving either the ACA and/or the corresponding pyridine ligands.[24,56,60] Likewise, the UV-vis spectra of the ligands and the reference L-tyrosine (L-tyr), as well as the absorption maxima (λ_{max}) and ε have also been recorded through the same methodology and are available in the ESI† (Table S3).

Photoluminescence. The emission spectra of all of the complexes and their corresponding ligands were obtained at 298 K, in MeOH (3-phpy, 2,2′-bipy, 1,10-phen and terpy ligands) or EtOH (complexes 1–6 and HACA, py, and mpterpy ligands), using the suitable concentrations extracted from the UV-vis data for the non-aggregated samples and irradiating each complex at their maximum excitation wavelength.

Considering that d^{10} metal compounds exhibit d orbitals with a closed shell configuration, only charge transfer (CT) transitions, either between the metal and the ligand (LMCT and MLCT) or by the ligand itself (LLCT), are allowed. Noteworthily, these CTs between π–π* orbitals are less energetic, and thus a bathochromic shift occurred.[61,62] The emission values for the six complexes increase in the order 1 < 3 < 4 < 2 < 5 < 6, presenting the maximum emission wavelengths between 331 and 395 nm (Fig. 8). In addition, compounds 1 and 5 show significant shoulders at 310 nm (1) and 314 and 340 nm (5), while the emission band of 2 and 6 extends until wavelengths above 450 nm. The resulting emission color ($\lambda_{max\text{-}em}$) for 1–6 lies in the blue region, according to the CIE1931 chromaticity diagrams.[63] The efficiency of the fluorescence emission of the complexes has been calculated using the fluorescence quantum yield (Φ), which is defined as the ratio of the number of photons emitted to the number of photons absorbed and describes how a fluorophore converts the excitation light into fluorescence.[64] The relative fluorescence quantum yield is calculated by relating the quantum yield value of the desired compound and comparing with a reference (standard).[65] The quantum yields of 1–6 are calculated using eqn (1),

$$\Phi_s = \Phi_r \left(\frac{OD_r}{OD_s}\right)\left(\frac{I_s}{I_r}\right)\left(\frac{n_s}{n_r}\right)^2 \quad (1)$$

where Φr and Φs are the quantum yields of the reference and the sample, respectively. I is the area under the curve of the emission spectra, OD is the optical density (or absorbance), and n is the refractive index of the solvent. Herein, L-tyrosine (L-tyr) was used as the standard (Φ_r = 0.14),[66] and the values of OD_r and I_r were obtained using a 2.21×10^{-6} M solution using Milli-Q water as a solvent (n_r = 1.3325),[67] at RT. The values of A_s and I_s of the ligands and 1–6 were recorded at 298 K using MeOH (n_s = 1.3314)[68] and EtOH (n_s = 1.3608)[69] as solvents, at concentrations detailed in the ESI† (Fig. S34–S39). Relevant parameters extracted from the photophysical properties of the free ligands are also provided in the ESI:† Table S3.

The values of relative quantum yields obtained for 1–6 are 0.13 (1), 0.065 (2), 0.023 (3), 0.029 (4), 0.058 (5) and 0.038 (6) (Table 4). Comparing these values with those of $[Zn(ACA)_2(H_2O)_2]$ and $[Zn(ACA)_2(4\text{-phpy})_2(H_2O)_2]\cdot 3H_2O$ obtained in previous publications (Φ = 0.019 and 0.00213, respectively),[36] complexes 1–6 present higher Φ values, probably because of the absence of coordinated water molecules, which provide additional pathways for nonradiative deactivation processes in comparison with pyridine ligands.[70] Noteworthily, the polymeric array of 1 presents a higher Φ with respect to the monomeric compounds 2–6, which is attributed to the higher rigidity of ACA in 1 produced by its bridging mode that connects the metal centers and ties up the acetamide moiety by the oxygen atom of their carbonyl group, permitting the energy transfer between the organic moieties to be maximized, and therefore, reducing the intraligand HOMO–LUMO gap.[71,72]

On the other hand, the monomeric complexes 2–6 present lower Φ values, with 2 being the most efficient probably due to the lower steric crowding of 3-phpy compared with the other pyridines in 3–6, which is evidenced by the symmetry of the metal core combined with their shorter bond lengths, with an average Zn–L value of 1.994 Å.[32] The Φ for 3 and 4 display similar values, which agree with similar outer atom angles of the 2,2′-bipy and 1,10-phen ligands. The subtle difference in their Φ values could be attributed to the higher torsion angle between the

rings of the 2,2′-bipy in 3 (7.64°), compared with those of the 1,10-phen in 4 (4a: 1.45°, 4b: 1.70°). The higher steric crowding of these N,N ligands, compared with the N donors in 1 and 2, results in an elongation of the Zn–L distances, with average values of 2.132 Å (3) and 2.116 (4), minimizing the CHEF and therefore, decreasing the Φ values.[73–76] This difference on the average Zn–L bond lengths could also be a factor which explains the higher Φ of 4 in comparison with 3. Finally, the Φ values of the N,N,N containing compounds (5 and 6) are different although they have similar outer atom angles, being higher for 5. These values could be associated with the higher degree of rotation of the 4′-(4-methylphenyl) moiety in 6 with respect to the higher rigidity of the terpy skeleton, which is shown in the structural section through the torsion angles between the aromatic rings of the terpy scaffold (3.67–5.73° for 5 and 6), compared with those of the 4′-(4-methylphenyl) moiety in 6 (21.69°).[77] For these compounds, the average Zn–L lengths of 2.048 (5) and 2.070 (6) show an intermediate elongation of the coordination bonds between the N and N,N donors, which is probably associated with the bidentate chelating coordination of the ACA in 3 and 4, resulting in six-coordinated species with higher steric crowding. This aspect combined with the presence of a double CHEF produced by the N,N,N ligands favors their higher Φ values compared with 3 and 4.

CONCLUSIONS

Six compounds have been synthesized by combining $Zn(OAc)_2{\cdot}2H_2O$, HACA and a comprehensive set of pyridine ligands based on their increasing denticity and steric crowding (N, N,N and N,N,N donors). From these reactions, one coordination polymer (1) and five monomeric complexes (2–6) were obtained. The use of N donor ligands with small steric crowding promotes the introduction of additional atoms such as the oxygen atom of the carbonyl group from the ACA (1) or the nitrogen atom from a second 3-phpy ligand (2), resulting in the formation of a coordination polymer and a monomer with a 1 : 1 ratio (ACA : dPy), respectively. Otherwise, when N,N and N, N,N donor ligands were used, monomeric complexes with general formula $[Zn(ACA)_2(dPy)]$ (3–6) were obtained. In all of them, the steric crowding produced by the introduction of bulkier dPy ligands has been evidenced through the coordination modes of the carboxylate groups, being bidentate chelate (3, 4a, and 4b) or monodentate (4a, 5, and 6) coordination modes. The elucidation of the crystal structures of 1–6 allows the study of their molecular and supramolecular interactions, observing the formation of four-coordinated (2), five-coordinated (1, 4a, 5, and 6) and six-coordinated (3, and 4b) species, which are associated mainly by π···π interactions and H-bonds via N–H···OOC and N–H···O=C interactions supported by weak C–H···O interactions. Furthermore, the UV-vis spectra were recorded, to observe the aggregation of the complexes at concentrations of $\sim 10^{-7}$ M through bathochromic shifts, corresponding to the formation of J-aggregates based on head-to-tail planar interactions. The photoluminescence properties of 1–6 have been measured at concentrations below aggregation and the Φ values have been calculated. The obtained values revealed that 1, presenting the ACA tied up through a bridging mode, shows the higher Φ, while for the monomeric forms 2–6 there is a competition between the favorable CHEF and the unfavorable effects of the steric crowding and the rotation capability of the dPy ligands. Finally, a larger contribution of the steric crowding over the CHEF has been observed, which results in higher Φ values for the N donor containing monomeric form (2) in comparison with the N,N and N,N,N donor containing forms (Φ order: 1 > 2 > 5 > 6 > 4 > 3). This study reflects the impact of the steric crowding generated by the ligands on the photophysical properties and stresses the guidelines to design new fluorescent coordination complexes.

EXPERIMENTAL SECTION

Synthesis of complexes 1–6

An EtOH solution (15 mL) of $Zn(OAc)_2{\cdot}2H2O$ (100 mg, 0.456 mmol) was added dropwise to a solution of HACA (187 mg, 0.912 mmol) and dPy (0.456 mmol), in EtOH (5 mL) as solvent at RT. The solution was stirred overnight until a white solid precipitated and then, it was kept in a freezer for one day. The resulting white solid was filtered, washed with 10 mL of cold Et_2O (repeated twice) and dried under vacuum. Furthermore, in the syntheses of 2 and 6, direct precipitation did not occur, and the obtained solution was concentrated under vacuum and kept in the fridge until a white solid (2) or an orange oil-like reaction crude (6) was obtained. In the case of 6, a resulting solid was obtained after forcing the precipitation of the orange oil using cold Et_2O. Further details about the characterization of 1–6 are available in the ESI.†

The synthesis of suitable crystals for X-ray diffraction was performed by different methods. For 1, the same synthetic methodology was used as for the synthesis of the solid but starting from 6.0 mg of $Zn(OAc)_2{\cdot}2H_2O$ and adding 2 mL of EtOH as the solvent, and the resulting solution was sealed and kept at RT for 5 days. For 2 and 4, the mother liquors were kept in the fridge at 4 °C for 7 (2) and 25 (4) days. For 3 and 5, the corresponding solids were recrystallized in EtOH (3) or DMF (5) and the resulting solutions were kept in the fridge at 4 °C for 5 days (3) or at RT for 2 days (5). Finally, for 6, a 2 mL solution of MeOH with the obtained solid was layered over 2 mL of heptane and the layering was kept at RT
for 7 days.

X-ray crystallographic data

For compounds 1–6, colorless prism-like samples were used for the X-ray crystallographic analysis. For the six compounds, the frames were integrated with the Bruker SAINT software package using a narrow-frame algorithm. All of the hydrogen atoms were refined using a riding model (AFIX) with an isotropic temperature factor equal to 1.2 and thus, the bond lengths of X–H were fixed (Tables 5 and 6). Further details about the crystal structure refinement are in the ESI.†

Conflicts of interest

There are no conflicts to declare.

ACKNOWLEDGMENTS

J. P. acknowledges financial support from the CB615921 project, the CB616406 project from "Fundació La Caixa", and the 2017SGR1687 project from the Generalitat de Catalunya. D. E. acknowledges the PIF predoctoral fellowship from the Universitat Autònoma de Barcelona.

REFERENCES

1 V. Sathish, A. Ramdass, M. Velayudham, K. L. Lu, P. Thanasekaran and S. Rajagopal, Dalton Trans., 2017, 46, 16738–16769.

2 H.-H. Cui, M.-M. Ding, X.-D. Zhang, W. Lv, Y.-Q. Zhang, X.-T. Chen, Z. Wang, Z.-W. Ouyang and Z.-L. Xue, Dalton Trans., 2020, 49, 14837–14846.

3 A. N. Gusev, M. A. Kiskin, E. V. Braga, M. Chapran, G. Wiosna-Salyga, G. V. Baryshnikov, V. A. Minaeva, B. F. Minaev, K. Ivaniuk, P. Stakhira, H. Ågren and W. Linert, J. Phys. Chem. C, 2019, 123, 11850–11859.

4 L.-L. Han, T.-P. Hu, K. Mei, Z.-M. Guo, C. Yin, Y.-X. Wang, J. Zheng, X.-P. Wang and D. Sun, Dalton Trans., 2015, 44, 6052–6061.

5 Y. Champouret, O. H. Hashmi and M. Visseaux, Coord. Chem. Rev., 2019, 390, 127–170.

6 X. Tian, S. Hussain, C. de Pace, L. Ruiz-Pérez and G. Battaglia, Chem. – Asian J., 2019, 14, 509–526.

7 Z. Xue, T. Sheng, Y. Wen, Y. Wang, S. Hu, R. Fu and X. Wu, CrystEngComm, 2015, 17, 598–603.

8 A. Lopera, A. Gil-Martínez, J. Pitarch-Jarque, B. Verdejo, S. Blasco, M. P. Clares, H. R. Jiménez and E. García-España, Dalton Trans., 2020, 49, 8614–8624.

9 C. Chen, S. M. Bellows and P. L. Holland, Dalton Trans., 2015, 44, 16654–16670.

10 C.-P. Li and M. Du, Chem. Commun., 2011, 47, 5958–5972.

11 I. M. L. Rosa, M. C. S. Costa, B. S. Vitto, L. Amorim, C. C. Correa, C. B. Pinheiro and A. C. Doriguetto, Cryst. Growth Des., 2016, 16, 1606–1616.

12 F. Yuan, J. Xie, H.-M. Hu, C.-M. Yuan, B. Xu, M.-L. Yang, F.-X. Dong and G.-L. Xue, CrystEngComm, 2013, 15, 1460–1467.

13 L. Bello, M. Quintero, A. J. Mora, T. González, A. Escalona, R. Añez, E. E. Ávila and A. Briceño, CrystEngComm, 2015, 17, 5921–5931.

14 A. Singh, P. Raj, J. J. Dubowski and N. Singh, Cryst. Growth Des., 2018, 18, 4320–4333.

15 M. Strianese, D. Guarnieri, M. Lamberti, A. Landi, A. Peluso and C. Pellecchia, Inorg. Chem., 2020, 59, 15977–15986.

16 W.-Y. Wong and C.-L. Ho, J. Mater. Chem., 2009, 19, 4457–4482.

17 R. Pandey, A. Kumar, Q. Xu and D. S. Pandey, Dalton Trans., 2020, 49, 542–568.

18 M. B. Rubin and S. E. Braslavsky, Photochem. Photobiol. Sci., 2010, 9, 670–674.

19 K. Khezami, K. Harmandar, E. Bağda, E. Bağda, G. Şahin, N. Karakodak, B. Jamoussi and M. Durmuş, J. Photochem. Photobiol., A, 2020, 401, 112736.

20 H. Ke, W. Wei, Y. Yang, H. Wu, Y.-Q. Zhang, G. Xie and S. Chen, Inorg. Chem., 2020, 59, 2833–2842.

21 F.-F. Chang, W.-Q. Li, F.-D. Feng and W. Huang, Inorg. Chem., 2019, 58, 7812–7821.

22 G. Volpi, E. Priola, C. Garino, A. Daolio, R. Rabezzana, P. Benzi, A. Giordana, E. Diana and R. Gobetto, Inorg. Chim. Acta, 2020, 509, 119662.

23 X.-M. Wang, S. Chen, R.-Q. Fan, F.-Q. Zhang and Y.-L. Yang, Dalton Trans., 2015, 44, 8107–8125.

24 A. Barbieri, G. Accorsi and N. Armaroli, Chem. Commun., 2008, 2185–2193.

25 J. Cepeda and A. Rodríguez-Diéguez, CrystEngComm, 2016, 18, 8556–8573.

26 M. D. Allendorf, C. A. Bauer, R. K. Bhakta and R. J. T. Houk, Chem. Soc. Rev., 2009, 38, 1330–1352.

27 D. Sun, Z.-H. Yan, V. A. Blatov, L. Wang and D.-F. Sun, Cryst. Growth Des., 2013, 13, 1277–1289.

28 D. Sun, M.-Z. Xu, S.-S. Liu, S. Yuan, H.-F. Lu, S.-Y. Feng and D.-F. Sun, Dalton Trans., 2013, 42, 12324.

29 R. D. Hancock, Chem. Soc. Rev., 2013, 42, 1500–1524.

30 G. Cheng, G. K.-M. So, W.-P. To, Y. Chen, C.-C. Kwok, C. Ma, X. Guan, X. Chang, W.-M. Kwok and C.-M. Che, Chem. Sci., 2015, 6, 4623–4635.

31 R. B. Martin, in Encyclopedia of Inorganic Chemistry, ed. R. B. King, John Wiley & Sons, Chichester, United Kingdom, 1994, vol. 46, p. 2195.

32 Y. Mikata, K. Kawata, S. Iwatsuki and H. Konno, Inorg. Chem., 2012, 51, 1859–1865.

33 Y. Mikata, Y. Nodomi, A. Kizu and H. Konno, Dalton Trans., 2014, 43, 1684–1690.

34 Z. Dai, Molecules, 2016, 21, 1647.

35 J. Soldevila-Sanmartín, T. Calvet, M. Font-Bardia, C. Domingo, J. A. Ayllón and J. Pons, Dalton Trans., 2018, 47, 6479–6493.

36 D. Ejarque, F. Sánchez-Férez, T. Calvet, M. Font-Bardia and J. Pons, Inorg. Chim. Acta, 2020, 509, 119695.

37 G. B. Deacon and R. J. Phillips, Coord. Chem. Rev., 1980, 33, 227–250.

38 K. Nakamoto, Infrared and Raman Spectra of Inorganic and Coordination Compounds: Part A: Theory and Applications in Inorganic Chemistry, Wiley Interscience, Hoboken, New Jersey, USA, 6th edn, 2009.

39 I. Fleming and D. Williams, Spectroscopic Methods in Organic Chemistry, Springer International Publishing, Cham, Switzerland, 7th edn, 2019.

40 D. Ejarque, T. Calvet, M. Font-Bardia and J. Pons, Molecules, 2020, 25, 3615.

41 A. W. Addison and T. N. Rao, J. Chem. Soc., Dalton Trans., 1984, 1349–1356.

42 S. Das and P. K. Bharadwaj, Cryst. Growth Des., 2006, 6, 187–192.

43 U. Pal Chaudhuri, L. R. Whiteaker, A. Mondal, E. L. Klein, D. R. Powell and R. P. Houser, Inorg. Chim. Acta, 2007, 360, 3610–3618.

44 N. Phukan and J. B. Baruah, RSC Adv., 2013, 3, 1151–1157.

45 L. Yang, D. R. Powell and R. P. Houser, Dalton Trans., 2007, 955–964.

46 P. M. Morse and G. S. Girolami, J. Am. Chem. Soc., 1989, 111, 4114–4116.

47 J. C. Friese, A. Krol, C. Puke, K. Kirschbaum and D. M. Giolando, Inorg. Chem., 2000, 39,

1496–1500.

48 F. Fernández-Palacio, J. Restrepo, S. Gálvez, P. Gómez-Sal and M. E. G. Mosquera, CrystEngComm, 2014, 16, 3376–3386.

49 A. Karmakar and J. B. Baruah, Polyhedron, 2008, 27, 3409–3416.

50 V. Viossat, P. Lemoine, E. Dayan, N. H. Dung and B. Viossat, J. Mol. Struct., 2005, 741, 45–52.

51 S. Naz, N. Uddin, K. Ullah, A. Haider, A. Gul, S. Faisal, A. Nadhman, M. Bibi, S. Yousuf and S. Ali, Inorg. Chim. Acta, 2020, 511, 119849.

52 S. A. Nikolaevskii, I. S. Evstifeev, M. A. Kiskin, A. A. Starikova, A. S. Goloveshkin, V. V. Novikov, N. V. Gogoleva, A. A. Sidorov and I. L. Eremenko, Polyhedron, 2018, 152, 61–72.

53 J. Jiang, J. Li, C. Liu, R. Liu, X. Liang, Y. Zhou, L. Pan, H. Chen and Z. Ma, JBIC, J. Biol. Inorg. Chem., 2020, 25, 311–324.

54 K. Prasad, R. Haldar and T. K. Maji, RSC Adv., 2015, 5, 74986–74993.

55 J. Nath, A. Tarai and J. B. Baruah, ACS Omega, 2019, 4, 18444–18455.

56 F. Sánchez-Férez, J. M. Rius-Bartra, T. Calvet, M. Font-Bardia and J. Pons, Inorg. Chem., 2021, 60, 3851–3870.

57 Y. Hong, J. W. Y. Lam and B. Z. Tang, Chem. Soc. Rev., 2011, 40, 5361–5388.

58 F. Würthner, T. E. Kaiser and C. R. Saha-Möller, Angew. Chem., Int. Ed., 2011, 50, 3376–3410.

59 M. Bayda, F. Dumoulin, G. L. Hug, J. Koput, R. Gorniak and A. Wojcik, Dalton Trans., 2017, 46, 1914–1926.

60 E. U. Mughal, M. Mirzaei, A. Sadiq, S. Fatima, A. Naseem, N. Naeem, N. Fatima, S. Kausar, A. A. Altaf, M. N. Zafar and B. A. Khan, R. Soc. Open Sci., 2020, 7, 201208.

61 J. E. Huheey, E. A. Keiter and R. L. Keiter, Inorganic chemistry: principles of structure and reactivity, HarperCollins College Publishers, New York, 4th edn, 1993.

62 D. Sutton, Electronic Spectra of Transition Metal Complexes, McGraw-Hill, London, UK, 1975.

63 T. E. Kokina, M. I. Rakhmanova, N. A. Shekhovtsov, L. A. Glinskaya, V. Y. Komarov, A. M. Agafontsev, A. Y. Baranov, P. E. Plyusnin, L. A. Sheludyakova, A. V. Tkachev and M. B. Bushuev, Dalton Trans., 2020, 49, 7552–7563.

64 M. E. Sommer, M. Elgeti, P. W. Hildebrand, M. Szczepek, K. P. Hofmann and P. Scheerer, in Methods in Enzymology, ed. A. K. Shukla, Elsevier Inc., Amsterdam, Netherlands, 1st edn, 2015

65 C. Würth, M. Grabolle, J. Pauli, M. Spieles and U. Resch-Genger, Nat. Protoc., 2013, 8, 1535–1550.

66 R. F. Chen, Anal. Lett., 1967, 1, 35–42.

67 G. M. Hale and M. R. Querry, Appl. Opt., 1973, 12, 555–563.

68 H. El-Kashef, Phys. B, 2000, 279, 295–301.

69 E. Sani and A. Dell'Oro, Opt. Mater., 2016, 60, 137–141.

70 F. W. Steuber, J. J. Gough, É. Whelan, L. Burtnyak, A. L. Bradley and W. Schmitt, Inorg. Chem., 2020, 59, 17244–17250.

71 Z. Wei, Z.-Y. Gu, R. K. Arvapally, Y.-P. Chen, R. N. McDougald, J. F. Ivy, A. A. Yakovenko, D. Feng, M. A. Omary and H.-C. Zhou, J. Am. Chem. Soc., 2014, 136, 8269–8276.

72 R.-P. Ye, X. Zhang, J.-Q. Zhai, Y.-Y. Qin, L. Zhang, Y.-G. Yao and J. Zhang, CrystEngComm, 2015, 17, 9155–9166.

73 N. J. Williams, W. Gan, J. H. Reibenspies and R. D. Hancock, Inorg. Chem., 2009, 48, 1407–1415.

74 D. Buist, N. J. Williams, J. H. Reibenspies and R. D. Hancock, Inorg. Chem., 2010, 49, 5033–5039.

75 D. Merrill, J. M. Harrington, H.-S. Lee and R. D. Hancock, Inorg. Chem., 2011, 50, 8348–8355.

76 H. Lee, H.-S. Lee, J. H. Reibenspies and R. D. Hancock, Inorg. Chem., 2012, 51, 10904–10915.

77 Z. Zhao, B. He and B. Z. Tang, Chem. Sci., 2015, 6, 5347–5365.

Table 1 Selected bond lengths (Å) and bond and twist angles (°) for 1–3

Complex 1	Bond lengths (Å)	Zn(1)–O(1)	1.972(2)	Zn(1)–O(5)	1.956(2)
		Zn(2)–O(2)	2.570(2)	Zn(1)–N(3)	2.122(3)
		Zn(1)–O(3)#1	2.010(2)		
	Bond angles (°)	O(1)–Zn(1)–O(2)	55.80(7)	O(2)–Zn(1)–N(3)	149.6(1)
		O(1)–Zn(1)–O(3)#1	118.54(8)	O(3)#1–Zn(1)–N(3)	100.1(1)
		O(1)–Zn(1)–N(3)	93.9(1)	O(5)–Zn(1)–O(1)	127.65(7)
		O(2)–Zn(1)–O(3)#1	94.32(7)	O(5)–Zn(1)–O(3)#1	99.41(7)
		O(2)–Zn(1)–O(5)	88.86(7)	O(5)–Zn(1)–N(3)	114.6(1)
	Symmetry operation	#1: $-x + 1/2, y - 1/2, -z + 3/2$			
Complex 2	Bond lengths (Å)	Zn(1)–O(1)	1.970(2)	Zn(1)–N(3)	2.018(2)
	Bond angles (°)	O(1)–Zn(1)–O(1)#1	98.3(1)	O(1)–Zn(1)–N(3)#1	114.17(8)
		O(1)–Zn(1)–N(1)	102.54(8)	N(3)–Zn(1)–N(3)#1	122.7(1)
	Symmetry operation	#1: $-x, y, -z + 1/2$			
Complex 3	Bond lengths (Å)	Zn(1)–O(1)	2.156(2)	Zn(1)–O(5)	2.177(3)
		Zn(1)–O(2)	2.148(2)	Zn(1)–N(3)	2.077(3)
		Zn(1)–O(4)	2.149(3)	Zn(1)–N(4)	2.089(3)
	Bond angles (°)	O(1)–Zn(1)–O(5)	151.8(1)	N(3)–Zn(1)–O(4)	152.9(1)
		O(2)–Zn(1)–O(1)	61.43(9)	N(3)–Zn(1)–O(5)	92.7(1)
		O(2)–Zn(1)–O(4)	98.0(1)	N(3)–Zn(1)–N(4)	78.6(1)
		O(2)–Zn(1)–O(5)	107.2(1)	N(4)–Zn(1)–O(1)	98.2(1)
		O(4)–Zn(1)–O(1)	93.66(9)	N(4)–Zn(1)–O(2)	155.1(1)
		O(4)–Zn(1)–O(5)	61.02(9)	N(4)–Zn(1)–O(4)	97.4(1)
		N(3)–Zn(1)–O(1)	113.4(1)	N(4)–Zn(1)–O(5)	97.3(1)
		N(3)–Zn(1)–O(2)	95.9(1)		
	Twist angles (°)	N(4)–Cg(1)–Cg(2)–N(3)	31.51	O(4)–Cg(1)–Cg(2)–O(5)	36.73
		O(1)–Cg(1)–Cg(2)–O(2)	27.09		

Table 2. Selected bond lengths (Å) and bond and twist angles (°) for 4–6

Complex 4	Bond lengths (Å)	Zn(1A)–O(1A)	2.316(4)	Zn(1B)–O(2B)	2.262(4)
		Zn(1A)–O(2A)	2.024(4)	Zn(1B)–O(4B)	2.143(4)
		Zn(1A)–O(4A)	1.960(4)	Zn(1B)–O(5B)	2.179(5)
		Zn(1A)–N(3A)	2.079(5)	Zn(1B)–N(3B)	2.070(5)
		Zn(1A)–N(4A)	2.091(5)	Zn(1B)–N(4B)	2.105(4)
		Zn(1B)–O(1B)	2.070(4)		
	Bond angles (°)	O(2A)–Zn(1A)–O(1A)	61.04(14)	O(1B)–Zn(1B)–N(3B)	116.7(2)
		O(2A)–Zn(1A)–N(3A)	122.4(2)	O(1B)–Zn(1B)–N(4B)	102.9(2)
		O(2A)–Zn(1A)–N(4A)	103.5(2)	O(4B)–Zn(1B)–O(2B)	95.7(2)
		O(4A)–Zn(1A)–O(1A)	98.5(2)	O(4B)–Zn(1B)–O(5B)	60.6(2)
		O(4A)–Zn(1A)–O(2A)	130.0(2)	O(5B)–Zn(1B)–O(2B)	109.5(2)
		O(4A)–Zn(1A)–N(3A)	102.0(2)	N(3B)–Zn(1B)–O(2B)	89.0(2)
		O(4A)–Zn(1A)–N(4A)	106.6(2)	N(3B)–Zn(1B)–O(4B)	94.0(2)
		N(3A)–Zn(1A)–O(1A)	92.3(2)	N(3B)–Zn(1B)–O(5B)	149.1(2)
		N(3A)–Zn(1A)–N(4A)	79.3(2)	N(3B)–Zn(1B)–N(4B)	79.3(2)
		N(4A)–Zn(1A)–O(1A)	154.6(2)	N(4B)–Zn(1B)–O(2B)	153.2(2)
		O(1B)–Zn(1B)–O(2B)	61.0(2)	N(4B)–Zn(1B)–O(4B)	109.1(2)
		O(1B)–Zn(1B)–O(4B)	139.2(2)	N(4B)–Zn(1B)–O(5B)	92.1(2)
		O(1B)–Zn(1B)–O(5B)	94.2(2)		
	Twist angles (°)	N(3B)–Cg(1)–Cg(2)–O(4B)	49.74	O(1B)–Cg(1)–Cg(2)–O(2B)	54.74
		N(4B)–Cg(1)–Cg(2)–O(5B)	35.56		
Complex 5	Bond lengths (Å)	Zn(1)–O(1)	1.975(2)	Zn(1)–N(3)	2.063(4)
		Zn(1)–N(2)	2.164(3)		
	Bond angles (°)	O(1)–Zn(1)–N(2)	97.4(1)	O(1)#1–Zn(1)–O(1)	99.2(1)
		O(1)–Zn(1)–N(3)	130.40(7)	N(2)#1–Zn(1)–N(2)	152.5(2)
		O(1)–Zn(1)–N(2)#1	100.4(1)	N(3)–Zn(1)–N(2)	76.23(7)
	Symmetry operation	#1: $-x, y, -z + 1/2$			
Complex 6	Bond lengths (Å)	Zn(1)–O(1)	1.982(2)	Zn(1)–N(4)	2.053(2)
		Zn(1)–O(4)	1.984(2)	Zn(1)–N(5)	2.157(3)
		Zn(1)–N(3)	2.174(3)		
	Bond angles (°)	O(1)–Zn(1)–O(4)	89.32(8)	O(4)–Zn(1)–N(4)	135.37(9)
		O(1)–Zn(1)–N(3)	98.57(9)	O(4)–Zn(1)–N(5)	101.06(9)
		O(1)–Zn(1)–N(4)	135.13(8)	N(4)–Zn(1)–N(3)	75.65(9)
		O(1)–Zn(1)–N(5)	102.71(9)	N(4)–Zn(1)–N(5)	76.41(9)
		O(4)–Zn(1)–N(3)	97.21(9)	N(5)–Zn(1)–N(3)	151.97(9)

Table 3. Structural parameters regarding the steric effects of the ligands in 1–6 and similar $Zn_{(II)}$ complexes containing ACA and dPy

Compound	Chelate angle ACA (°)	Bite angle dPy (°)	Outer atom angle[56] (°)	Ref.
1	55.80	—	80.19	This work
2	—	—	94.19	This work
3	61.01, 61.43	78.63	154.60	This work
4a	61.08	79.28	153.22	This work
4b	60.56, 60.92	79.32	153.41	
5	—	76.22, 76.22	226.01	This work
6	—	75.66, 76.39	226.36	This work
$[Zn_2(\mu\text{-}O,O'\text{-}ACA)_2(ACA)_2(4\text{-}Phpy)_2]_n$	—	—	80.86, 80.53	39
$[Zn_3(\mu\text{-}ACA)_6(4\text{-}Phpy)_2]\cdot 4CH_3CN$	124.48–125.98	—	82.42	39
$[Zn(ACA)_2(4\text{-}phpy)_2(H_2O)_2]\cdot 3H_2O$	—	—	79.42	31

Table 4. Detailed parameters extracted from the photoluminescence properties of 1–6 and similar $Zn_{(II)}$ complexes containing ACA and dPy[a]

Sample	$\lambda_{max\text{-}Abs}$ (log(ε))	λ_{ex}	$\lambda_{max\text{-}em}$	Φ_s
1	201 (4.60), 278 (4.55)	234	338	0.13
2	202 (5.01), 273 (4.85)	231	339	0.065
3	202 (4.97), 244 (4.69), 280 (4.92)	232	336	0.023
4	201 (5.19), 271 (5.31)	232	338	0.029
5	201 (4.89), 272 (4.83)	232	331	0.058
6	201 (4.99), 279 (5.00)	294	395	0.038
$[Zn(ACA)_2(H_2O)_2]$	207 (5.37), 279 (4.80)	275	343	0.019
$[Zn(ACA)_2(4\text{-phpy})_2(H_2O)_2]\cdot 3H_2O$	203 (6.20), 261 (4.51)	275	342	0.0021

[a] All the wavelengths are given in nm. ε values are given in M^{-1} cm^{-1}. $\lambda_{max\text{-}Abs}$ = maximum of absorption. $\lambda_{max\text{-}em}$ = maximum of emission. Φ_s = quantum yield.

Table 5 Crystal data and structure refinement for 1–3

	1	2	3
Empirical formula	$C_{27}H_{25}N_3O_6Zn$	$C_{46}H_{44}N_4O_7Zn$	$C_{40}H_{52}N_4O_{10}Zn$
Formula weight	552.87	830.22	814.22
T (K)	100(2)	100(2)	100(2)
Wavelength (Å)	0.71073	0.71073	0.71073
System, space group	Monoclinic, $P2_1/n$	Monoclinic, $C2/c$	Monoclinic, $P2_1/c$
Unit cell dimensions			
a (Å)	14.0509(7)	31.098(3)	16.763(2)
b (Å)	10.1555(5)	5.7198(4)	15.886(2)
c (Å)	17.930(1)	23.853(2)	16.337(2)
α (°)	90	90	90
β (°)	103.030(2)	106.322(4)	108.155(4)
γ (°)	90	90	90
V (Å^3)	2492.7(2)	4071.3(6)	4134.1(9)
Z	4	4	4
D_{calc} (mg m^{-3})	1.473	1.354	1.308
μ (mm^{-1})	1.033	0.660	0.654
F (000)	1144	1736	1720
Crystal size (mm^{-3})	0.350 × 0.280 × 0.240	0.142 × 0.066 × 0.065	0.450 × 0.300 × 0.090
hkl ranges	$-20 \leqq h \leqq 19$, $0 \leqq k \leqq 14$, $0 \leqq l \leqq 25$	$-44 \leqq h \leqq 44$, $-8 \leqq k \leqq 8$, $-33 \leqq l \leqq 34$	$-20 \leqq h \leqq 20$, $-19 \leqq k \leqq 19$, $-20 \leqq l \leqq 20$
θ range (°)	2.320 to 30.585	2.529 to 30.563	2.459 to 26.498
Reflections collected/unique/[R_{int}]	7618/7618/0.0477	37 250/6212/0.0667	52 003/8520/0.1237
Completeness to θ (%)	99.7	99.8	99.9
Absorption correction	Semi-empirical from equivalents	Semi-empirical from equivalents	Semi-empirical from equivalents
Max. and min. transmission	0.7461 and 0.6269	0.7461 and 0.6814	0.7454 and 0.5569
Refinement method	Full-matrix least-squares on F^2	Full-matrix least-squares on F^2	Full-matrix least-squares on F^2
Data/restraints/parameters	7618/6/306	6212/3/265	8520/0/503
Goodness-on-fit on F^2	1.049	1.040	1.021
Final R indices [$I > 2\sigma(I)$]	R_1 = 0.0559, wR_2 = 0.1422	R_1 = 0.0601, wR_2 = 0.1325	R_1 = 0.0564, wR_2 = 0.1332
R indices (all data)	R_1 = 0.0670, wR_2 = 0.1521	R_1 = 0.0871, wR_2 = 0.1499	R_1 = 0.0996, wR_2 = 0.1600
Extinction coefficient	n/a	n/a	n/a
Largest diff. peak and hole (e Å^{-3})	2.036 and −1.609	1.221 and −1.575	0.893 and −1.115

Table 6. Crystal data and structure refinement for 4–6

	4	5	6
Empirical formula	$C_{74}H_{74}N_8O_{15}Zn_2$	$C_{43}H_{45}N_7O_8Zn$	$C_{48}H_{53}N_5O_{10}Zn$
Formula weight	1446.15	853.23	925.32
T (K)	100(2)	100(2)	100(2)
Wavelength (Å)	0.71073	0.71073	0.71073
System, space group	Orthorhombic, $Pca2_1$	Monoclinic, $C2/c$	Triclinic, $P\bar{1}$
Unit cell dimensions			
a (Å)	16.8072(9)	33.183(7)	11.8153(9)
b (Å)	16.4259(8)	8.925(2)	12.280(1)
c (Å)	24.761(2)	15.409(3)	17.493(2)
α (°)	90	90	108.449(4)
β (°)	90	115.059(8)	96.437(4)
γ (°)	90	90	102.812(4)
V (Å^3)	6835.7(6)	4133.8(2)	2301.7(3)
Z	4	4	2
D_{calc} (mg m^{-3})	1.405	1.371	1.335
μ (mm^{-1})	0.776	0.656	0.597
F (000)	3016	1784	972
Crystal size (mm^{-3})	0.776 × 0.130 × 0.042	0.260 × 0.130 × 0.040	0.150 × 0.100 × 0.080
hkl ranges	$-20 \leqq h \leqq 23$, $-23 \leqq k \leqq 22$, $-34 \leqq l \leqq 34$	$-47 \leqq h \leqq 47$, $-12 \leqq k \leqq 12$, $-20 \leqq l \leqq 22$	$-16 \leqq h \leqq 16$, $-17 \leqq k \leqq 17$, $-25 \leqq l \leqq 24$
θ range (°)	2.390 to 30.058	2.381 to 30.624	1.982 to 30.665
Reflections collected/unique/[R_{int}]	66 762/19 837/0.1300	45 954/6337/0.1001	66 736/14 116/0.0774
Completeness to θ (%)	99.9	99.9	99.9
Absorption correction	Semi-empirical from equivalents	Semi-empirical from equivalents	Semi-empirical from equivalents
Max. and min. transmission	0.7448 and 0.6580	0.7461 and 0.6052	0.7461 and 0.6182
Refinement method	Full-matrix least-squares on F^2	Full-matrix least-squares on F^2	Full-matrix least-squares on F^2
Data/restraints/parameters	19 837/1/899	6337/5/315	14 116/1/586
Goodness-on-fit on F^2	0.920	1.059	1.054
Final R indices [$I > 2\sigma(I)$]	R_1 = 0.0415, wR_2 = 0.0739	R_1 = 0.0763, wR_2 = 0.1496	R_1 = 0.0631, wR_2 = 0.1551
R indices (all data)	R_1 = 0.1321, wR_2 = 0.1085	R_1 = 0.1230, wR_2 = 0.1701	R_1 = 0.1056, wR_2 = 0.1849
Extinction coefficient	n/a	n/a	n/a
Largest diff. peak and hole (e Å^{-3})	2.095 and −0.946	1.313 and −1.046	1.396 and −0.969

FIGURE CAPTIONS

Scheme 1. Outline of the synthesis of complexes 1–6.

Figure 1. a) Molecular structure of 1 along the bc plane. (b) Detailed view of the intramolecular interactions. General view of the supramolecular contacts expanding the structure through: (c) the [101] direction and (d) a direction. Some atoms which do not participate in any intermolecular interactions have been omitted for clarity.

Figure 2. Metal cores of the monomeric species: (a) 2, (b) 3, (c) 4a, (d) 4b, (e) 5, (f) 6.

Figure 3. a) Supramolecular b directed chains of 2 with a detailed view of the formed N–H···O$_{COO}$ and C–H···O interactions. (b) 2D supramolecular plane formed along the ac plane with a detailed view of the C–H···π interactions. Some atoms which do not participate in any intermolecular interactions have been omitted for clarity in the detailed views.

Figure 4. (a and b) Detailed views of the N–H···OCOO, C–H···O and $\pi\cdots\pi$ interactions propagating the structure of 3 in the b axis. (c) General view of the supramolecular ($10\bar{1}$) plane. (d) Detailed view of the O–H···O and N–H···O interactions Involving the occluded EtOH molecules. (e) General view of the 1D chain formed along the c axis. Some atoms which do not participate in any intermolecular interactions have been omitted for clarity in the detailed views and (e).

Figure 5. (a and b) Detailed views of the supramolecular interactions expanding the structure of 4 along the b axis. (c) General view of the supramolecular bc plane. Detailed views of: (d and e) the H-bonds involving the occluded EtOH molecules which expand the structure along the c direction. (f) $\pi\cdots\pi$ interactions expanding the structure along the a axis. (g) General view of the supramolecular chain formed along the a axis. Some atoms which do not participate in any intermolecular interactions have been omitted for clarity in the detailed views.

Figure 6. General views of the supramolecular chains of 5 formed along: (a) the b axis and (b) c axis.

Figure 7. (a) General view of the supramolecular chain of 6 along the [220] direction. (b and c) Detailed views of the supramolecular structures along the [220] chain. (d) General view of the supramolecular (002) plane. (e) Detailed view of the role of the MeOH molecules joining the monomeric units in the c direction. Some atoms which do not participate in any intermolecular interactions have been omitted for clarity in the detailed views.

Figure 8. Emission spectra of complexes 1–6, excited at 234 nm (1), 231 nm (2), 232 nm (3–5) and 294 nm (6) at 298 K in EtOH solutions (3.54×10^{-7} M for 1, 4.05×10^{-7} M for 2, 5.24×10^{-8} M for 3, 1.50×10^{-8} M for 4, 7.39×10^{-8} M for 5 and 3.43×10^{-8} M for 6).

Scheme 1

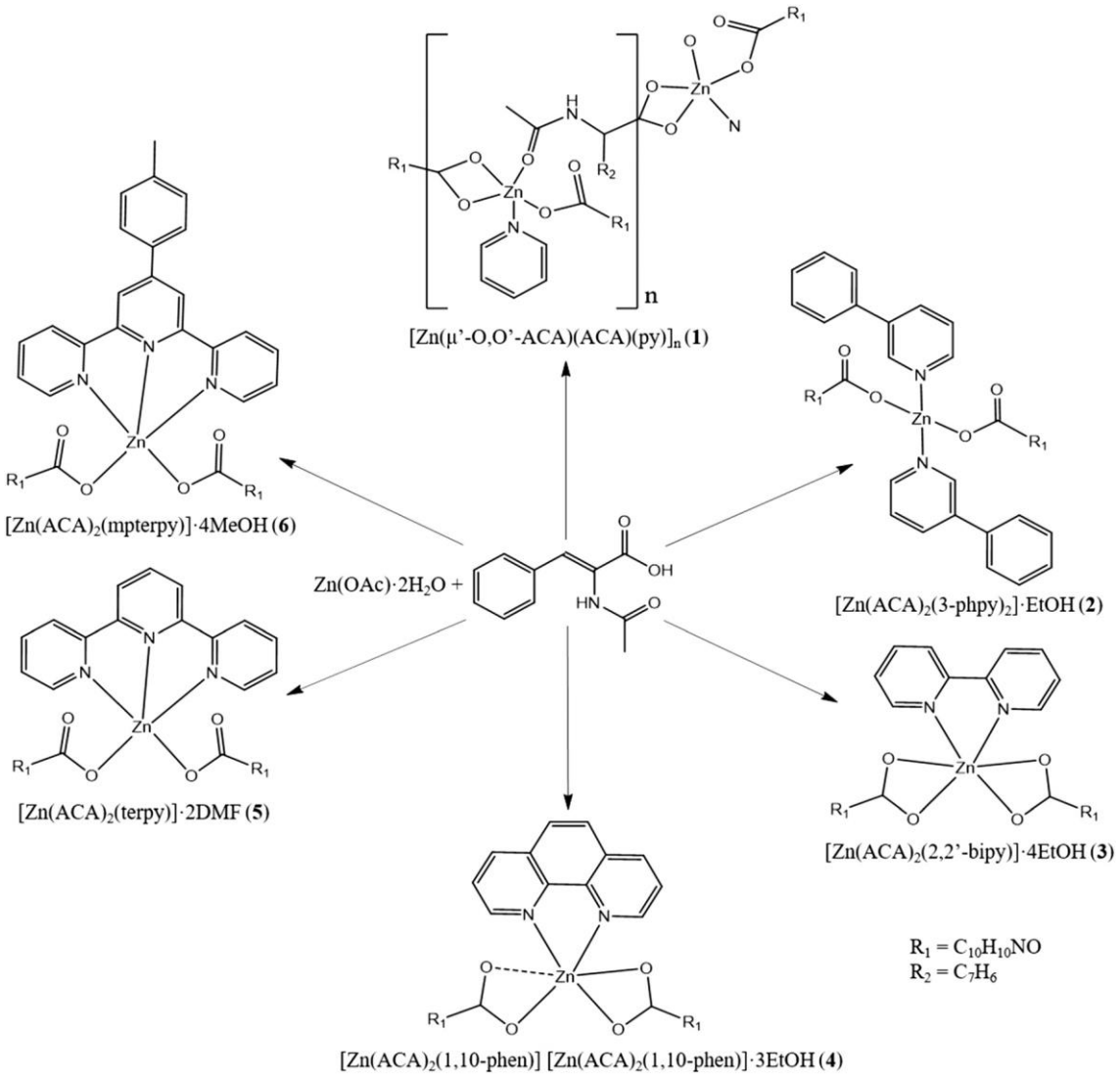
[Zn(μ'-O,O'-ACA)(ACA)(py)]n (1)
[Zn(ACA)2(mpterpy)]·4MeOH (6)
[Zn(ACA)2(3-phpy)2]·EtOH (2)
Zn(OAc)·2H2O +
[Zn(ACA)2(terpy)]·2DMF (5)
[Zn(ACA)2(2,2'-bipy)]·4EtOH (3)
[Zn(ACA)2(1,10-phen)] [Zn(ACA)2(1,10-phen)]·3EtOH (4)
R1 = C10H10NO
R2 = C7H6

Figure 1.

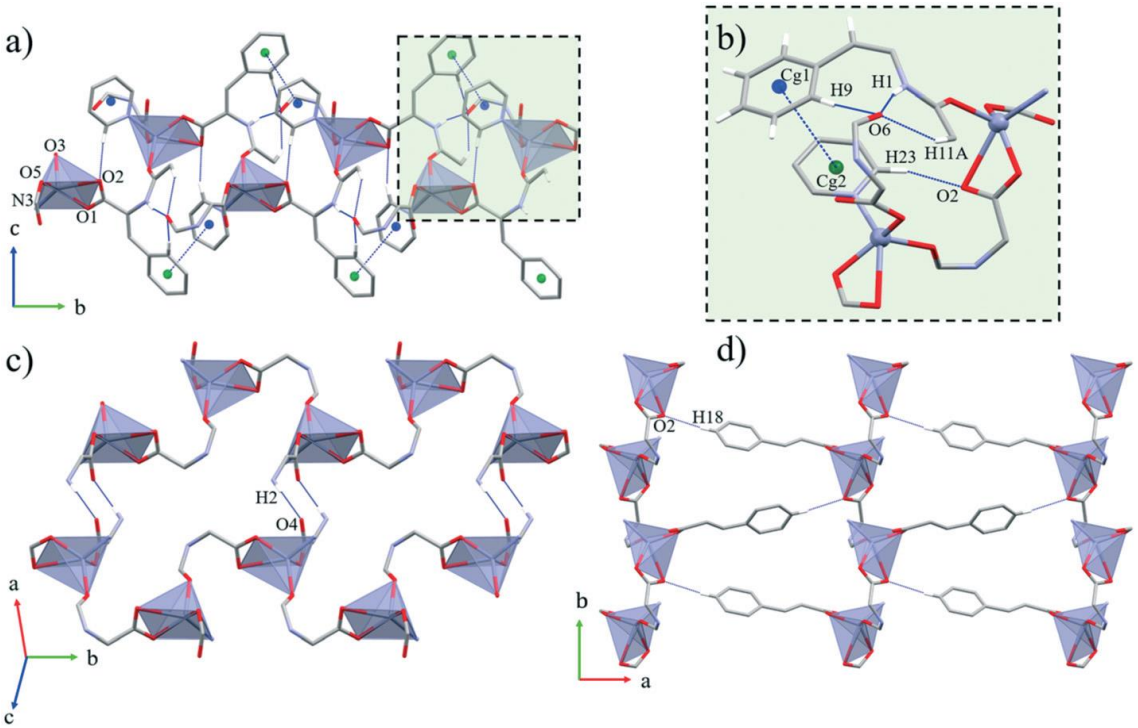
a)
O3
O5
O2
N3
O1
c
b
b)
Cg1
H9
H1
O6
H23
H11A
Cg2
O2
c)
H2
O4
a
b
c
d)
O2
H18
b
a

Figure 2.

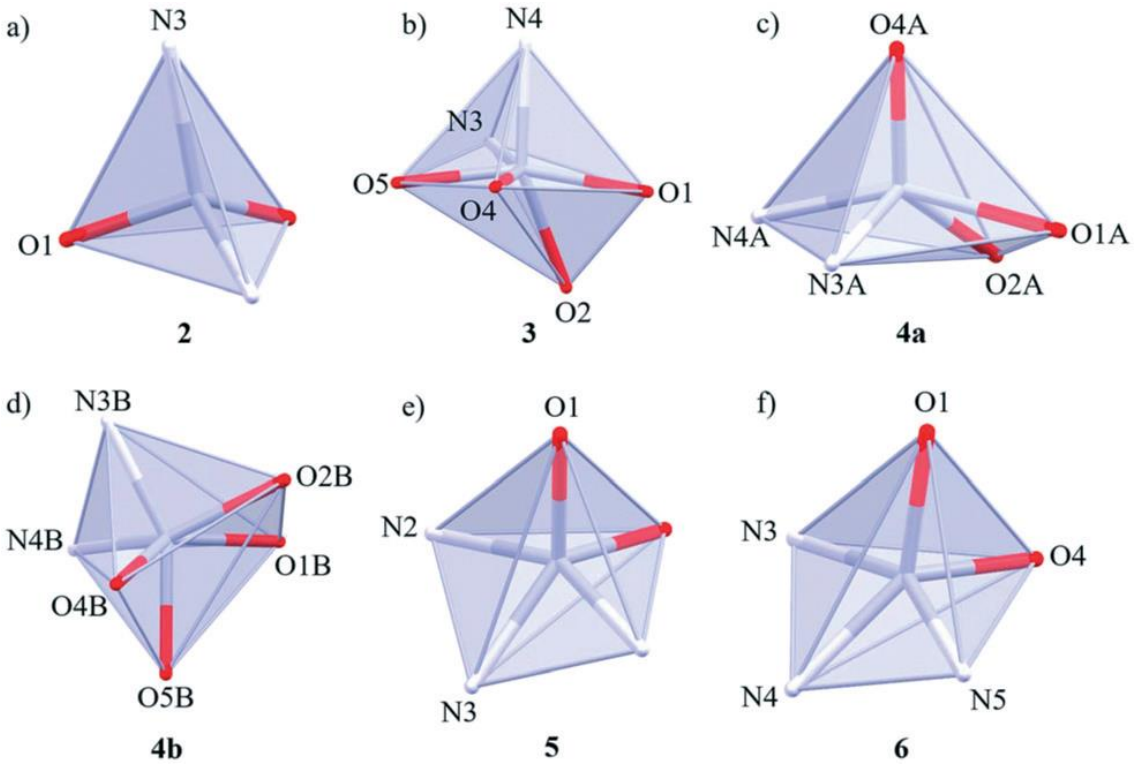
a)
N3
O1
2
b)
N4
N3
O5
O4
O1
O2
3
c)
O4A
N4A
O1A
N3A
O2A
4a
d)
N3B
O2B
N4B
O1B
O4B
O5B
4b
e)
O1
N2
N3
5
f)
O1
N3
O4
N4
N5
6

Figure 3

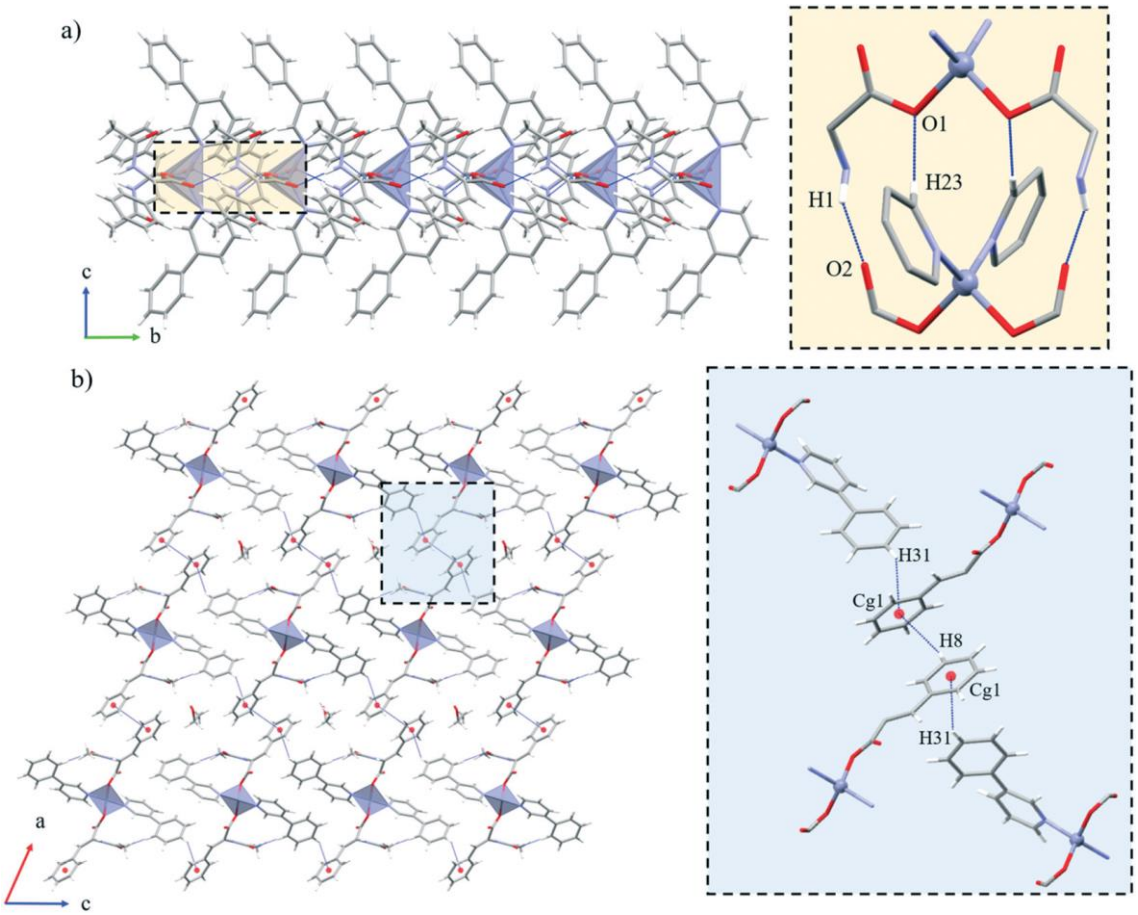

Figure 4

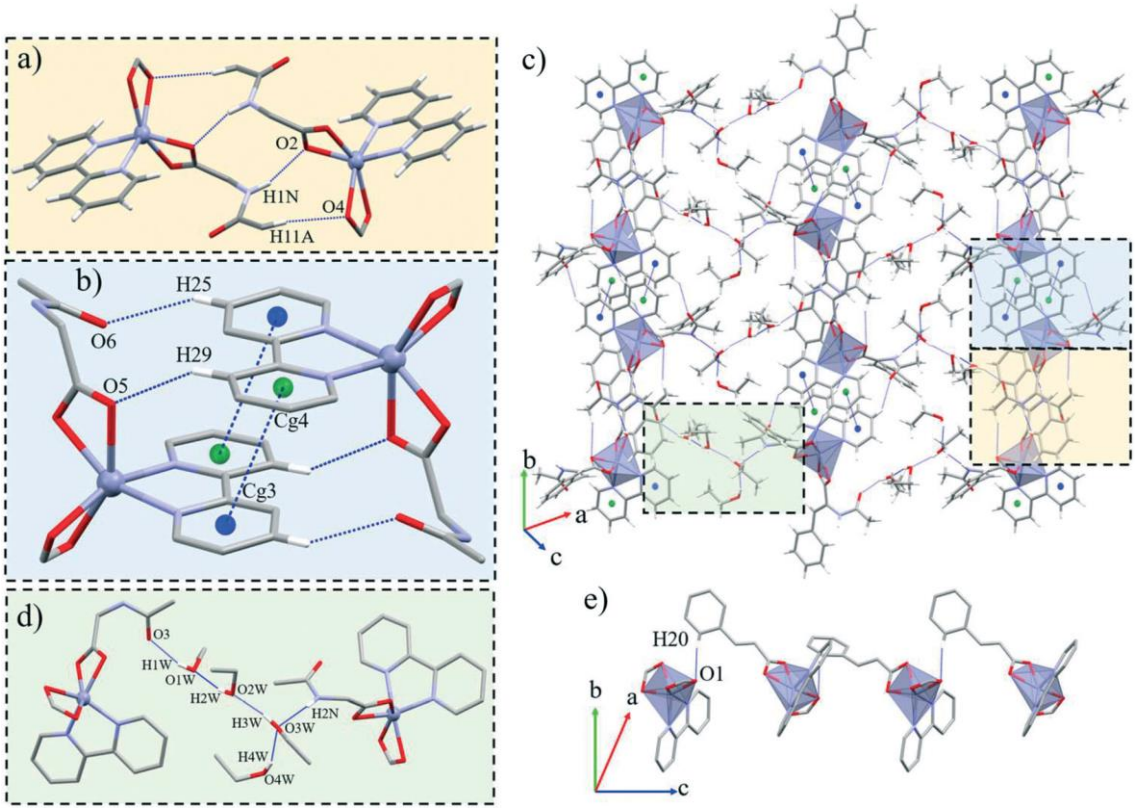
a)
O2
H1N
O4
H11A
b)
H25
O6
H29
O5
Cg4
Cg3
c)
b
a
c
d)
O3
H1W
O1W
H2W
O2W
H3W
O3W
H2N
H4W
O4W
e)
H20
O1
b
a
c

Figure 5

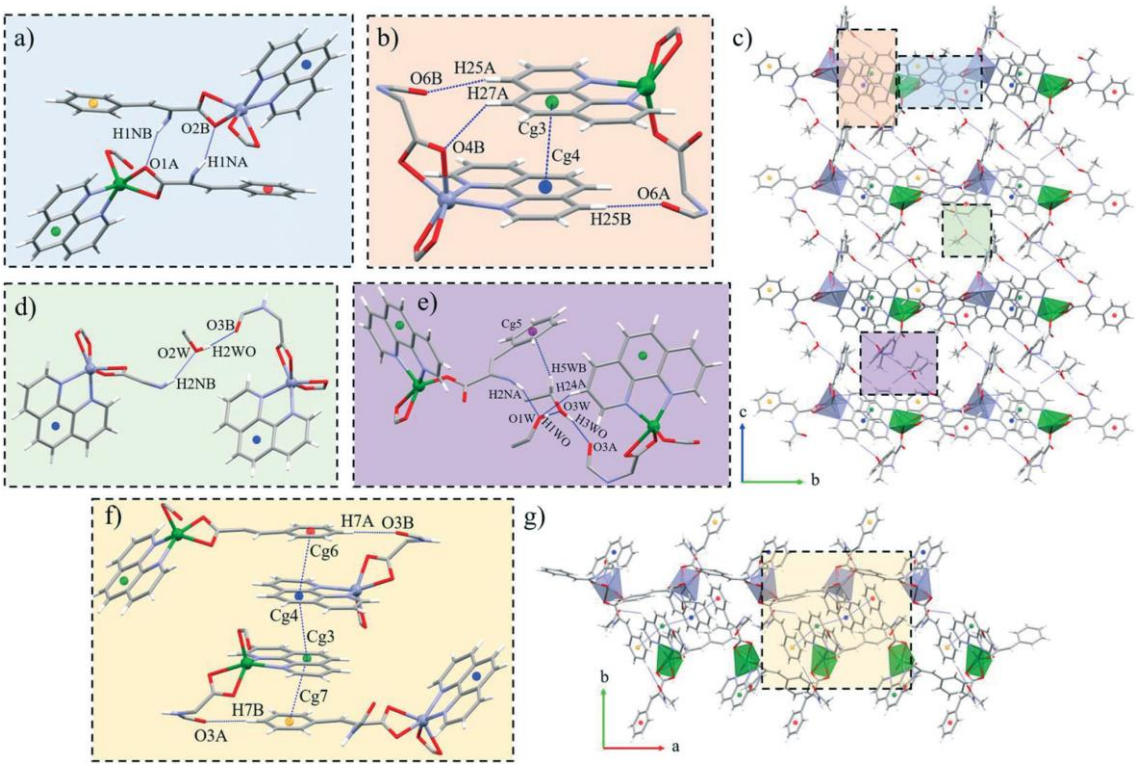
a)
H1NB
O2B
O1A
H1NA
b)
O6B
H25A
H27A
Cg3
O4B
Cg4
O6A
H25B
c)
c
b
d)
O3B
O2W
H2WO
H2NB
e)
Cg5
H5WB
H24A
H2NA
O3W
O1W
H1WO
H3WO
O3A
f)
H7A
O3B
Cg6
Cg4
Cg3
Cg7
H7B
O3A
g)
b
a

Figure 6

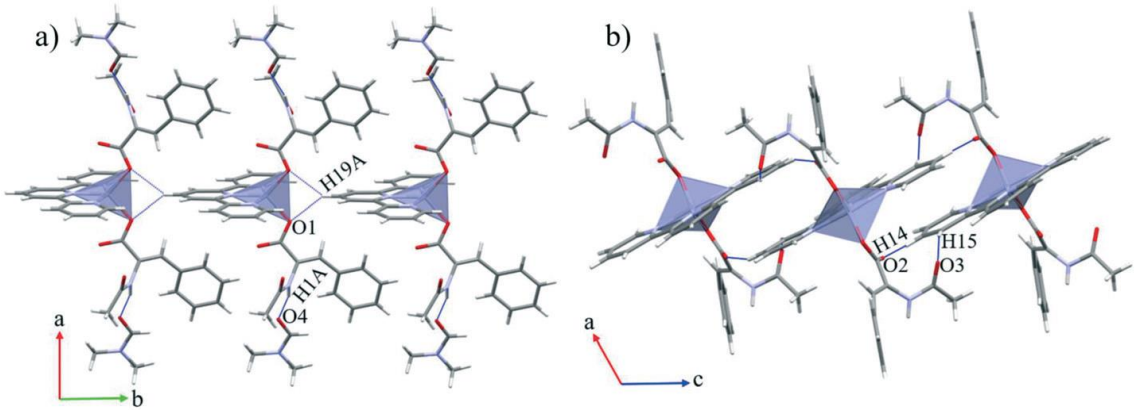

Figure 7

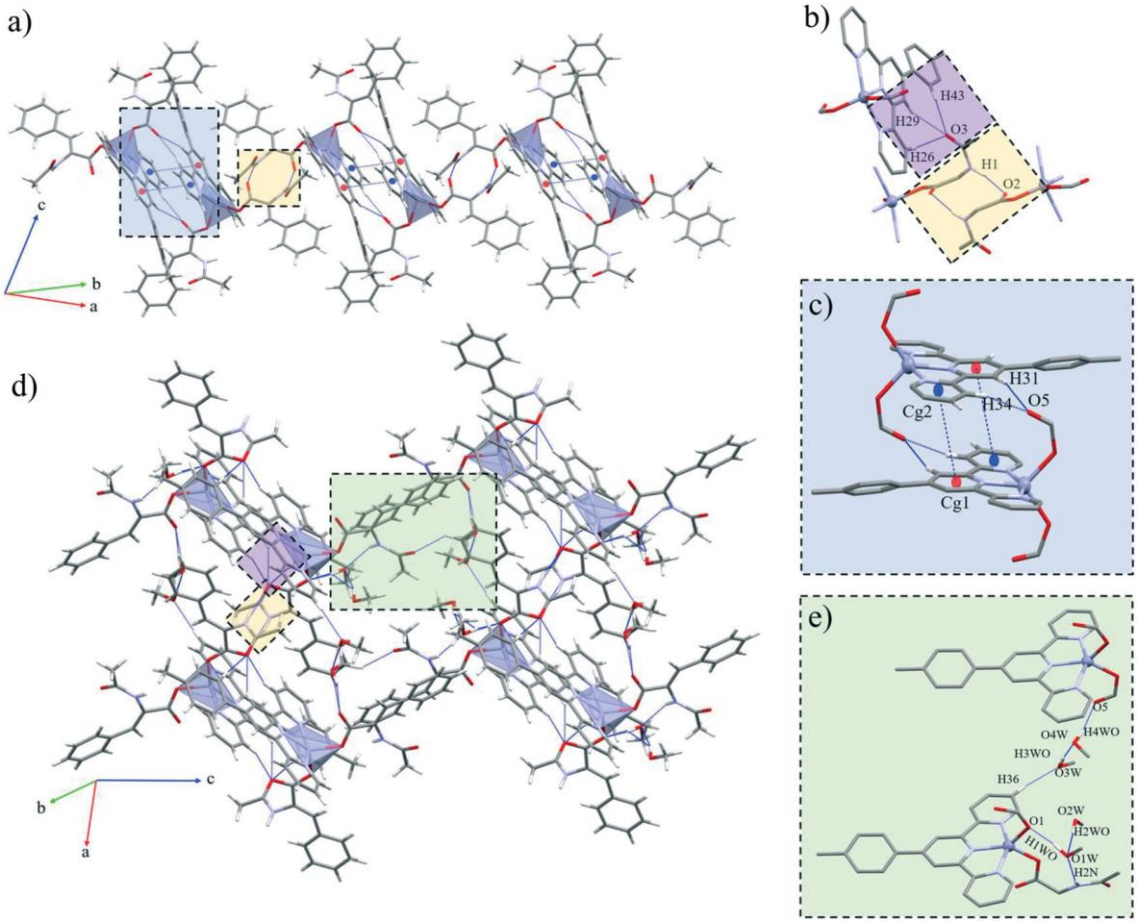
a)
c
b
a
b)
H43
H29
O3
H26
H1
O2
c)
H31
Cg2
H34
O5
Cg1
d)
b
c
a
e)
O5
O4W
H4WO
H3WO
O3W
H36
O2W
O1
H2WO
H1WO
O1W
H2N

Figure 8

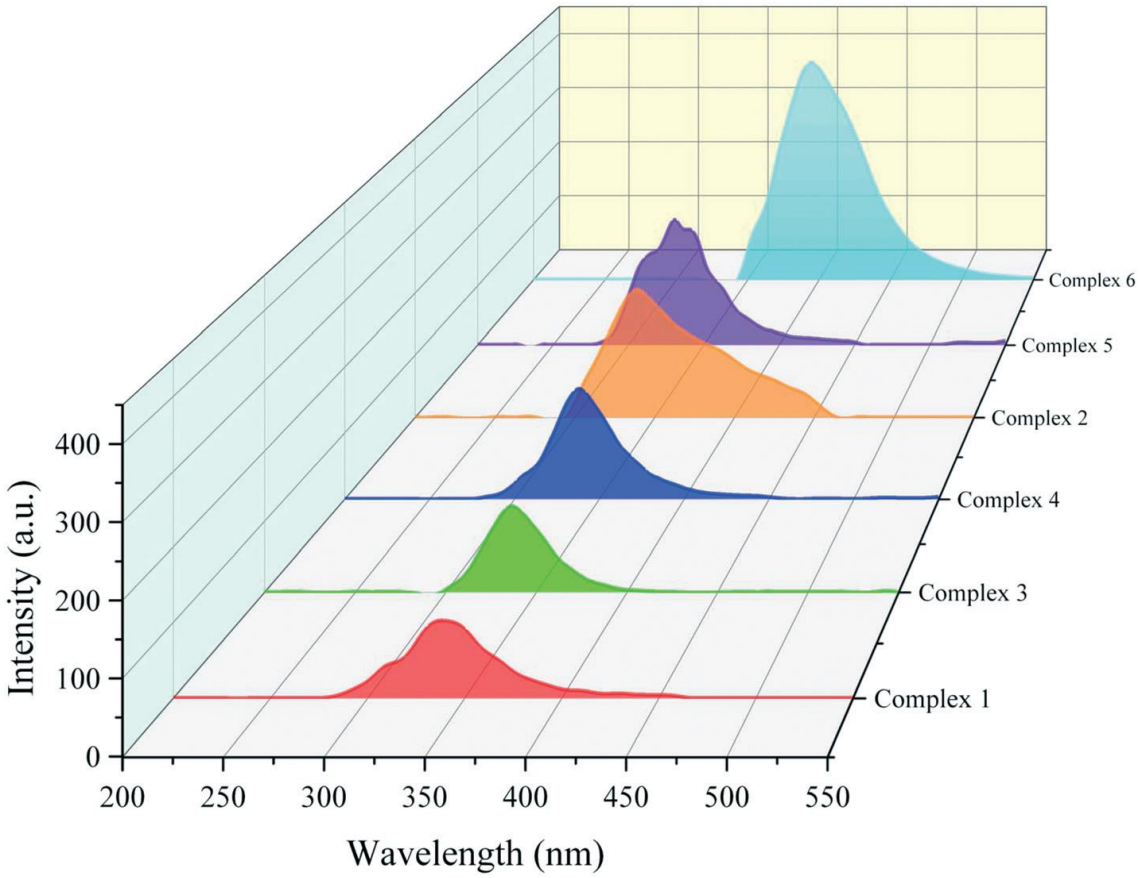
Complex 6
Complex 5
Complex 2
Complex 4
Complex 3
Complex 1
Intensity (a.u.)
0
100
200
300
400
200
250
300
350
400
450
500
550
Wavelength (nm)